Special Issue

Eletrônica de Potência
Open Journal of Power Electronics

Received April 29, 2025; accepted July 31, 2025; Date of publication August 15, 2025.
The review of this paper was arranged by Associate Editor Roberto F. Coelho and Editor-in-Chief Telles B. Lazzarin

Digital Object Identifier http://doi.org/10.18618/REP.e202546

Advanced Monitoring and Control Strategies for Off-Grid Water Pumping Systems

Luis A. G. Lopes[1,2], Giovani A. Castro[1], Diuary Gonçalves[2,3], Renata O. de Sousa[4], Allan F. Cupertino[5], Heverton A. Pereira[1]

[1]Federal University of Viçosa, Department of Electrical Engineering, Viçosa, MG, Brazil.
[2]Centro Federal de Educação Tecnológica de Minas Gerais, Department of Electrical Engineering, Belo Horizonte, MG, Brazil.
[3]Centro Federal de Educação Tecnológica Celso Suckow da Fonseca,Department of Electrical Engineering, Nova Friburgo, RJ, Brazil
[4]Federal University of Technology – Parana, Department of Electronics, Curitiba, PR, Brazil.
[5]Federal University of Juiz de Fora, Department of Electrical Energy, Juiz de Fora, MG, Brazil.

e-mail: luis.a.lopes@ufv.br; giovani.castro@ufv.br; diuary.goncalves@ufv.br; renatasousa@utfpr.edu.br; allan.cupertino@ufjf.br; heverton.pereira@ufv.br.
*Corresponding author.

ABSTRACT

The growing demand for energy in remote and isolated regions, where access to the conventional electrical system is limited, has been driving the development of off-grid systems. A common type of off-grid power system employs photovoltaic systems associated with battery banks. However, these systems face challenges due to their remote location and their reliance on weather conditions for energy generation. Furthermore, it is crucial that these systems can communicate operational discrepancies, notify maintenance teams, and receive commands to activate energy-saving modes during adverse weather conditions. This work presents a simple and cost-effective approach to enhance the operation of an off-grid system, transforming it from a conventional system into an intelligent operation using the cloud-based platform known as "thingable!". The results highlight a cloud interface creation that enables the control of a pumping system. This interface is enabled by monitoring operational parameters, such as voltage, IGBTs temperature, and power delivered. To validate the proposed changes, a monitoring test was carried out using a controlled pump from 9:10 a.m. to 10:10 a.m., powered by an inverter connected to a 100 V DC bus. Additionally, a test was conducted to assess the pump behavior under a fixed duty cycle of 60%.

KEYWORDS off-grid system, Internet of Things, photovoltaic system, hydraulic pump.

I. INTRODUCTION

Over the years, the importance of electrical energy has grown rapidly due to its role as a basic resource in industrial production, service sector and commerce in general, in addition to providing comfort to homes [1], [2]. Nevertheless, according to the International Energy Agency (IEA), 760 million people still lack access to energy, most of those people located in rural regions of developing countries [3], [4]. In these areas, the lack of a centralized distribution network has made it difficult for communities to access electricity, and network expansion is often expensive [5]. Alongside this, another challenge to a sustainable future is to provide a secure energy supply with a lower impact on climate change [1].

In this context, the off-grid energy system has become increasingly important in providing viable electricity solutions. Moreover, the off-grid photovoltaic solar energy system has emerged as a sustainable and autonomous solution to meet the energy needs of remote areas and places where conventional electrical infrastructure is limited or nonexistent [4], [6], [7]. The photovoltaic energy systems generate electrical energy from sunlight based on photovoltaic panels. Due to the intermittency of this energy source, battery energy storage systems (BESS) are usually employed, to ensure uninterrupted power supply to the connected loads during weather conditions changes [8]. Therefore, through these systems it is possible to meet the energy demands of these remote areas, ensuring sustainable energy access [5], [9].

Although the benefits of off-grid photovoltaic systems, the design and control of these systems require a tailored and applied approach to meet the specific needs of each installation [6], [9]–[11]. The integration of advanced control, monitoring and energy storage technologies has a key role in overcoming this challenge [12]. In addition, the off-grid photovoltaic systems based on battery energy storage systems require controlling a battery bank charger, usually based on a DC-DC converter, and an inverter, if alternating current (ac) is required by the installation loads, as illustrated in Fig. 1. Moreover, due to the unavailability of the electrical grid (off-grid), two requirements must be met for real-time operation of an off-grid system: power balance between generation and load demand, and control of voltage amplitude and frequency of the installation [13].

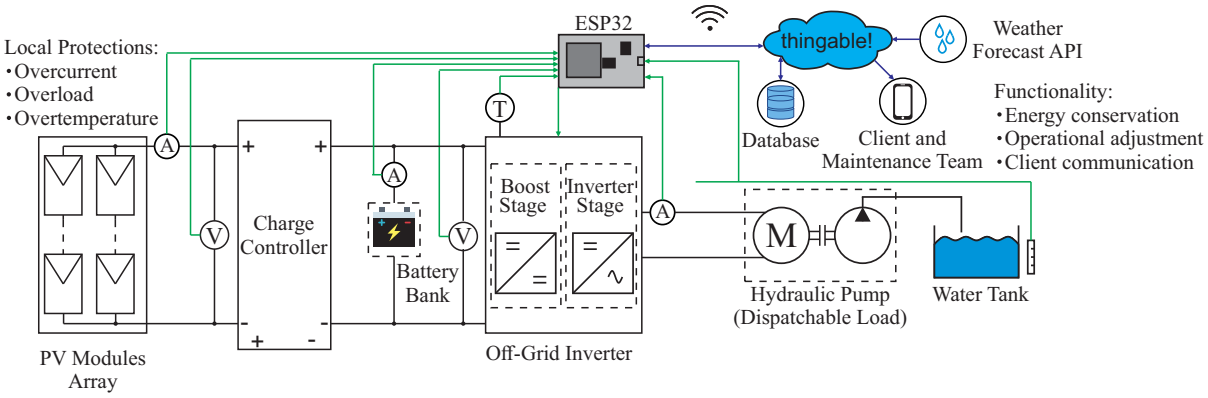

FIGURE 1. An off-grid system integrated with the cloud *thingable!* platform.

In this context, the Internet of Things (IoT) technology can gain prominence in the control, automation, and monitoring of off-grid photovoltaic energy systems [12], [14]. This technology is capable of connecting physical devices and objects in the real world to the internet, allowing them to collect and share data, communicate with each other, and, in many cases, take autonomous actions based on the collected data [14], [15].

The use of smart off-grid systems implemented in base stations can prevent energy outages by forecasting energy demand in advance. This is done by taking into account the available power of the base stations, the usage of different transmission methods, and the state of charge of the battery pack [16], [17]. Other systems may employ an on/off-grid switch. In case of disconnection, the smart system isolates from the grid, manages the local energy, and distributes it to the local loads [18].

By integrating intelligent agents capable of sending and receiving data, it is possible to optimize energy consumption. The assistance of an intelligent operator can determine the optimal use of multiple energy sources, thus maximizing energy efficiency [19], [20]. Additionally, the prediction of weather and load behavior can enhance the adaptability of the off-grid system. By connecting to an external agent, the system can leverage predictive capabilities to anticipate future requirements and optimize its operations accordingly [21], [22].

Therefore, considering the increased interest in IoT-enabled smart energy grid systems, this paper proposes a low-cost wireless controlled and monitored off-grid system, which is a continuation of the work proposed in [23]. In the previous work, an off-grid system communication is based on an ESP-32 microcontroller which communicates wirelessly with the *thingable!* platform was developed. In this system, the data acquired from the system sensors are sent wirelessly through microcontroller to the *thingable!* platform, where the data can be processed and storaged [24]. In addition to the previous work, the control commands can be sent through the *thingable!* platform to the microcontroller to perform the wireless control of the smart off-grid system. Furthermore, this work introduces a methodology for using data of the pump parameterization for the control tuning aimed at regulating water flow. This approach allows for precise and efficient control of the off-grid system, facilitating the analysis of the collected data and allowing direct actions according to the commands of the platform.

This paper is organized as follows. In Section II, the considered control for the converters and pump are considered. Section III outlines the case study. Section IV presents results and discussion. Conclusions are provided in Section V.

II. CONTROL STRATEGY

This section showcases the control strategy implemented at each stage of the system. The parameters for the control tunning are shown in Table 1 in Section III.

A. Off-Grid System and IoT Network

Fig. 1 shows a smart off-grid system. It presents a photovoltaic (PV) panel connected to a charger controller. The charger controller regulates the power supplied to DC loads within the installation. Additionally, it connects the batteries with the inverters. The inverter powers a hydraulic pump to fill the water tank. The pump functions as a dispatchable load.

The ESP32 microcontroller has the function of controlling the on-site operations. It is responsible for monitoring various parameters, which includes the IGBTs temperature, measured through sensors built-in in the IGBT module, the load voltage and current readings, as well as the water flow level. This data allows the microcontroller to control the inverter operation through square wave signals sent to the IGBTs gate-drives. Furthermore, the system protection includes over-temperature, overload, and overcurrent functions. These protective measures contribute to maintaining the safety of the system.

In addition, the ESP32 microcontroller enables data transmission to and from the *thingable!* platform using Message Queuing Telemetry Transport (MQTT) protocol. The *thingable!* platform serves as an online platform specifically designed for advanced applications within an Internet of

Things (IoT) network. It enables data storage in the cloud, enabling further analysis that goes beyond the capabilities of the on-site microcontroller and advanced decision-making capabilities.

Furthermore, the platform has the capability to alert clients or maintenance teams regarding any anomalies or improper functioning of the off-grid installation. This early warning system allows the predictions of potential failures, thus preventing catastrophic accidents. When failure occurs, the platform facilitates a better understanding of the root causes, making it easier to address and correct the issues.

The implemented strategies in the system are adjusted based on additional applications integrated into the *thingable!* platform. For instance, accessing the application programming interface (API) for weather forecast allows the smart use of weather information to predict scenarios where energy conservation becomes necessary. By anticipating weather conditions that may lead to insufficient energy generation, the system can make smart adjustments in your operation to ensure the client does not experience power shortages during unfavorable weather conditions. Or during the dry season, the smart off-grid system can leverage any rainfall to ensure the tank maintains its maximum water level.

B. Charger Controller

To maximize the energy efficiency of a photovoltaic module, a converter is required to regulate its input power. Since the module's power output has a maximum point, a maximum power point tracking (MPPT) algorithm can be implemented. The system using a buck converter is shown in Figure 2. Where the photovoltaic module is represented by an equivalent constant voltage source (V_{eq}) and equivalent resistance (R_{eq}). A capacitor is connected in the module output, with capacitance (C_{pv}) and equivalent series resistance (R_c), and an inductor in the output with inductance of (L_{pv}) and resistance (R_{pv}) in the battery bank with voltage (v_{bat}).

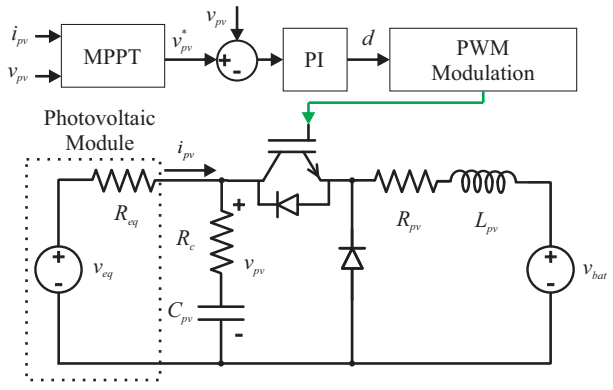

FIGURE 2. Buck converter used to connect the photovoltaic module to the battery bank.

Furthermore, the control is based on [25], [26], where the plant transfer function is derived from the relationship between the photovoltaic module voltage and the converter duty cycle. Accordingly :

$$G_{vd}(s) = \frac{\hat{v}_{pv}}{\hat{d}} = \frac{A\,(sC + A)}{\left(I_L + V_{pv}DA\left(\frac{1}{R_L} + \frac{sL}{B}\right)\right)\left(\frac{1}{R_{eq}} + \frac{D^2}{B}\right)} \tag{1}$$

where $A = 1 + sCR_C$ and $B = R_L + sL$. The equation considers the average values under the nominal operating conditions of the converter. Thus, V_{pv} corresponds to the expected value photovoltaic module nominal voltage, D is the expected duty cycle, and I_L represents the expected inductor current.

The control tuning must ensure a cut-off frequency higher than the capacitor-related value $\omega_{pv} = 1/(C_{pv}R_c)$ to avoid operating in the critical zone [25]. Operating in this region results in a low phase margin, which may lead to instability. Furthermore, the control is tuned to ensure that the cut-off frequency is not placed in this region. For this plant, a PI controller is considered for implementation, given by:

$$G_{pi,buck,i} = K_{p,pv} + \frac{K_{i,pv}}{s}. \tag{2}$$

the gains were adjusted to have a cut-off frequency of $\omega_{pv}/10$, resulting in a proportional gain $(K_{p,pv} = 0.6863)$ and the integral gain $(K_{i,pv} = 22.87)$. Furthermore, the open-loop transfer function is shown in Figure 3.

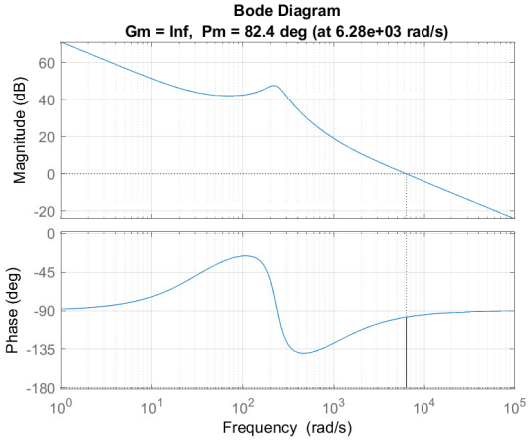

FIGURE 3. Buck converter open loop transfer function with the PI control transfer function.

C. Boost control

Furthermore, a bidirectional boost converter is placed at the inverter's input to raise the battery voltage to the required DC-link levels. This connection integrates the battery with the MPPT-controlled buck converter and the solar panel. The boost converter setup is shown in Figure 4. Where v_{bat} is the nominal battery bank voltage, i_{bat} is its current, L_{bat} is the inductor used in the filter, and R_{bat} is its resistance. C_{dc} represents the DC-link capacitance, and R_{dc} corresponds to the nominal power of the system.

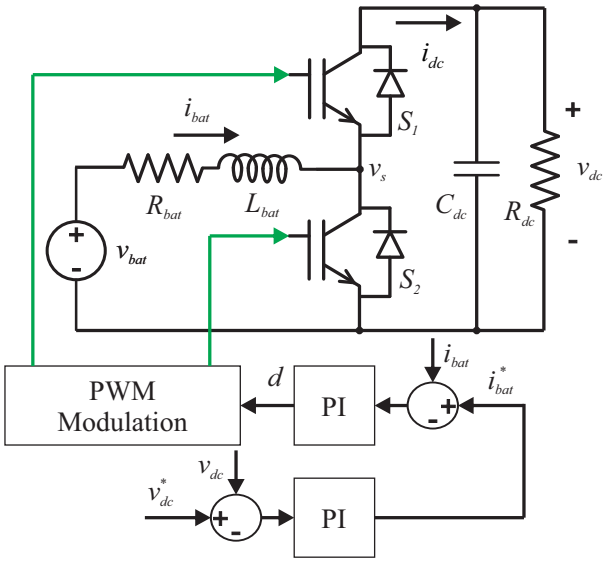

FIGURE 4. Boost converter, used to connect the input of the inverter to the battery bank.

In this converter, the switches S_1 and S_2 are complementary, meaning when one is closed, the other is open. Let v_s denote the average voltage across S_2, which depends on the duty cycle d, the DC-link voltage v_{dc}, and the current drawn from the DC-link i_{dc}. Over one switching period T_s, during the interval dT_s, switch S_1 is closed and $v_s = v_{dc}$; during the remaining interval $(1-d)T_s$, S_2 is closed and $v_s = 0$. Therefore, the average value of v_s can be expressed as:

$$\bar{v}_s = dv_{dc}. \tag{3}$$

Furthermore, the same principle can be applied to the current. During dT_s, when S_1 is closed, $i_{dc} = i_{bat}$, and during $(1-d)T_s$, when S_2 is closed, $i_{dc} = 0$. Therefore, the average value of i_{dc} can be expressed as:

$$\bar{i}_{dc} = di_{bat}. \tag{4}$$

Furthermore, considering the average behavior of the system and taking into account the inductor and capacitor, two equations can be derived from it:

$$v_{bat} - \bar{v}_s = v_{bat} - dv_{dc} = i_{bat}(L_{bat}s + R_{bat}), \tag{5}$$

$$i_{dc} = di_{bat} = v_{dc}(C_{dc}s + \frac{1}{R_{dc}}). \tag{6}$$

The selected control for this system is a cascade control, where the inner loop controls i_{bat}, and the outer loop controls v_{dc}. The output of the inner control is dv_{dc}, and the plant transfer function can be obtained from equation 5. By considering v_{bat} as a disturbance, and for obtaining the plant transfer function, it is disregarded is:

$$G_{p,boost,i} = -\frac{i_{bat}}{dv_{dc}} = \frac{1}{(L_{bat}s + R_{bat})}, \tag{7}$$

where the value of d can be normilized by $\frac{1}{v_{dc}}$ to obtain d for modulation. Furthermore, a PI controller is implemented in this loop, given by:

$$G_{pi,boost,i} = K_{p,boost,i} + \frac{K_{i,boost,i}}{s}. \tag{8}$$

For the controller parameter tuning, the pole cancellation technique is used, with the cut-off frequency allocated as $f_{boost,i} = \frac{f_{sw,boost}}{20}$, where $f_{sw,boost}$ is the switching frequency. This results in the following gains [27]:

$$K_{p,boost,i} = -2\pi f_{boost,i} L_{bat}, \tag{9}$$

$$K_{i,boost,i} = K_{p,boost,i}\frac{R_{bat}}{L_{bat}}. \tag{10}$$

Furthermore, for the outer loop control, it is assumed that the inner control loop is much faster than the outer loop, which can be adjusted by tuning the cut-off frequency to $f_{boost,v} = \frac{f_{boost,i}}{20}$. This control regulates the DC-link voltage, with v_{dc} as the input and the output being the reference for the inner control, i_{bat}. The plant transfer function can be obtained from equation 6, considering i_{dc} as a disturbance and setting it to zero for modeling:

$$G_{p,boost,v} = \frac{v_{dc}}{i_{bat}} = \frac{d}{(C_{dc}s + \frac{1}{R_{dc}})}, \tag{11}$$

where in this case, the duty cycle is considered at its average value of operation, approximately $d \approx 1 - \frac{v_{bat}}{v_{dc}}$, accounting for the voltage drop across the resistance.

Furthermore, for the outer control loop, a PI controller is also used, while being tuned using pole allocation [27] and given by:

$$G_{pi,boost,v} = K_{p,boost,v} + \frac{K_{i,boost,v}}{s}. \tag{12}$$

Considering the plant transfer function of the boost converter between the DC-link voltage and the battery current, as given in equation 11, and the PI controller transfer function defined in equation 12, the controller gains are determined using the pole placement technique, resulting in:

$$K_{p,boost,v} = 2\pi f_{boost,c} C_{dc} d, \tag{13}$$

$$K_{i,boost,v} = \frac{K_{p,boost,v}}{C_{dc}R_{dc}}. \tag{14}$$

D. Flow control

By using the first Ziegler-Nichols method, also known as the *reaction curve method* or *open-loop method*, it is possible to tune a PI controller based on the step response of the system. This approach consists of applying a step input to the plant in open-loop configuration and analyzing the resulting output curve, which should resemble an S-shaped response. From this response, three key parameters are extracted:

- K: the steady-state gain, calculated as the ratio between the change in output and the amplitude of the step input;
- L: the apparent time delay, determined by extrapolating the tangent at the inflection point of the curve until it intersects the time axis;
- T: the time constant, estimated by the time between the tangent's intersection with the time axis and the point where it reaches the steady-state value.

Using these parameters, the plant can be approximated by a first-order system with time delay, known as the FOPDT (First-Order Plus Dead Time) model, represented as:

$$G(s) = \frac{Ke^{-Ls}}{Ts+1}. \tag{15}$$

The PI controller is then designed using empirical formulas proposed by Ziegler and Nichols:

$$k_p = 0.9 \cdot \frac{T}{L}, \qquad T_i = \frac{L}{0.3}$$

$$C(s) = k_p\left(1 + \frac{1}{T_i s}\right). \tag{16}$$

From the step response shown in Figure 5, the following values were obtained:

$$T = 0.2, \quad L = 0.055, \quad K = \frac{0.3387}{0.9} = 0.3763$$

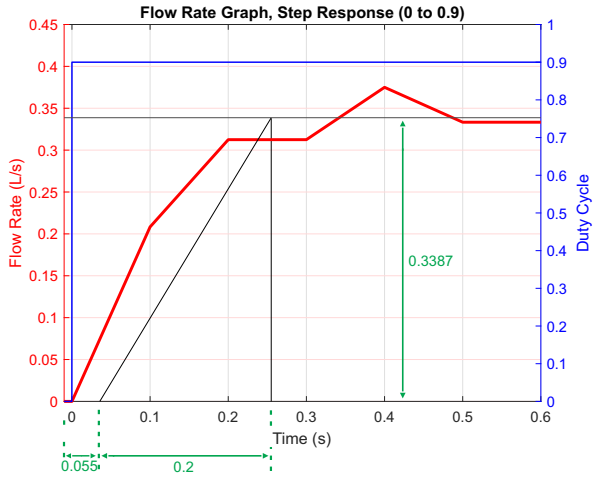

FIGURE 5. Flow rate graph — Step response from 0 to 0.9

Applying the tuning formulas with the extracted parameters results in the following transfer functions for the plant and the controller:

$$G(s) = \frac{0.3763e^{-0.055s}}{0.2s+1} \tag{17}$$

$$C(s) = 3.2727 + \frac{17.8512}{s} \tag{18}$$

Therefore, the plant and controller transfer functions become:

$$G(s) = \frac{0.3763e^{-0.055s}}{0.2s+1}. \tag{19}$$

$$C(s) = 3.2727 + \frac{17.8512}{s}. \tag{20}$$

Consequently, the resulting closed-loop system is:

$$G_{closed}(s) = \frac{-0.2258s^2 + 6.979s + 44.79}{0.03667s^3 + 1.291s^2 + 13.65s + 281.944.79}. \tag{21}$$

Finally, the Bode diagram of the open-loop system is presented, highlighting the gain and phase margins, which demonstrate the stability of the system.

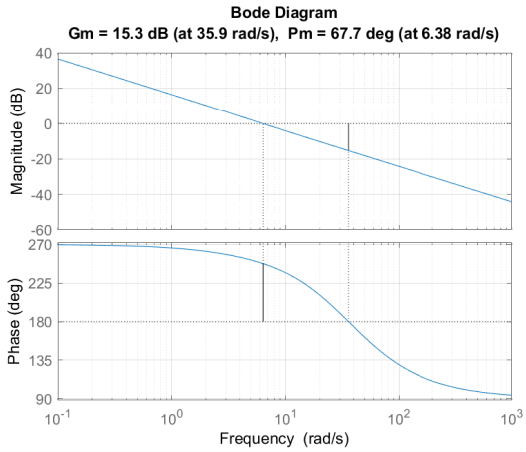

FIGURE 6. Bode Diagram of the Open-Loop System

To implement the control algorithm on a digital platform, specifically an ESP32 microcontroller, it was necessary to discretize the continuous-time PI controller. Digital controllers operate in discrete time and require the transformation of continuous-domain transfer functions into equivalent discrete-time representations that preserve the system dynamics as closely as possible.

The discretization method used in this study is the Tustin method. This method approximates the continuous derivative through a transformation that replaces the variable s with the variable z, with the relationship between these variables expressed as:

$$s \approx \frac{2}{T} \cdot \frac{1 - z^{-1}}{1 + z^{-1}}, \tag{22}$$

where T is the sampling period. In this study, a sampling period of 100 ms was adopted for the application of the method. Resulting in the closed-loop system.

$$G_{closed}(z) = \frac{0.3049z^4 - 0.06264z^3 - 0.2557z^2 + ...}{z^5 - 1.678z^4 + 1.009z^3 + ... \\ ... + 0.1148z - 0.002847 \\ \hline ... + 0.2563z^2 + 0.02403z - 0.0004728}. \tag{23}$$

Finally, the unit step response of the system is presented below.

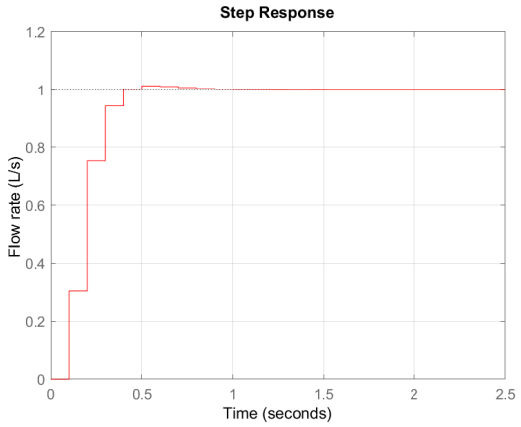

FIGURE 7. Unit Step Response of the Closed-Loop System

E. Single-phase Inverter

The inverter topology considered in this study is shown in Figure 8.

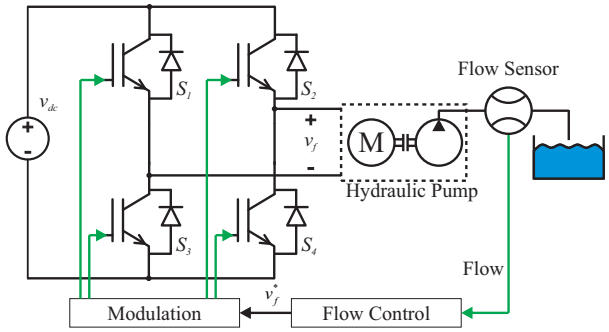

FIGURE 8. Single-phase inverter topology employed to drive the pump.

It consists of a single-phase full-bridge inverter using four IGBTs. A modified square-wave modulation scheme is employed, where a zero-voltage interval is introduced within each cycle [28]. This modification enables control over the inverter output voltage amplitude, allowing flow regulation as described in Section D. The flow control strategy provides the modulation block with a voltage reference signal, denoted as v_f^*, which then determines the desired inverter output voltage v_f.

III. CASE STUDY

This section introduces the test bench and simulation case used to validate the system. Furthermore, IoT integration is also shown.

A. Thingable! Interface

The control and monitoring of the system, performed through the application designer available in *thingable!*, enable the development of advanced applications with a user interface that provides both control signals and real-time data visualization of monitored variables. Additionally, the system integrates an API to retrieve weather forecasts, including precipitation predictions for the upcoming days. Fig. 9 shows the implemented interface.

In this interface, the top-left corner displays the pump control commands, along with a forecast of precipitation for the next seven days, solar radiation levels, estimated generated energy, and the projected available state of charge (SOC). The SOC estimation considers the energy generation and the standard pump consumption behavior. All data is retrieved via an API [29]. Moreover, a Clear button is provided to reset the displayed data.

Adjacent to the control panel, an indicator displays the average SOC levels predicted for the next days of operation. These predictions are based on the pump's past behavior and the estimated energy generation.

B. Test Bench

Fig. 10 shows the experimental setup. The system uses a single-phase inverter, ac 100-240 Vrms, DC voltage: 400 V or below, that employs an IGBT module from Mitsubishi Electric, part number PSS15S92F6-AG, rated at 15 A and 600 V. IGBTs were chosen over MOSFETs due to their suitability for higher voltage levels. This setup was selected to allow for broader, more general applications across different voltage and power ranges, even though the case study does not require it. The DC-link has a total capacitance of 1690 µF. It is connected to a DC source, simulating the DC side, operating at 100 V. The selected capacitors are electrolytic capacitors. The inverter is connected to a submerged hydraulic pump. The ESP32 transmits two square wave signals with a frequency of 50 Hz, one for each arm of the inverter. The voltage signal is controlled based on commands sent by the broker, where the duty cycle is adjusted as needed.

A performance test of the system is considered to evaluate its communication with the *thingable!* platform and its response. In this test, a command is sent from the cloud platform to the ESP32, enabling modification of the voltage reference and changing the current output of the inverter.

When a command is sent, the power delivery to the pump is adjusted, regulating the water flow rate. Then, an experiment was conducted to measure the time it takes to fill a 25-liter container to estimate the relationship between these parameters. The container was positioned 1 meter above the water level and connected via a flexible silicone tube with an $1/2$-inch internal diameter. This relationship is illustrated in Fig. 11.

Additionally, the temperature parameters of the IGBTs, ambient temperature, and DC voltage are measured through the ports of the ESP32 microcontroller. Furthermore, the temperature of the switches and the DC-link voltage are provided by sensors integrated into the inverter board. Mean-

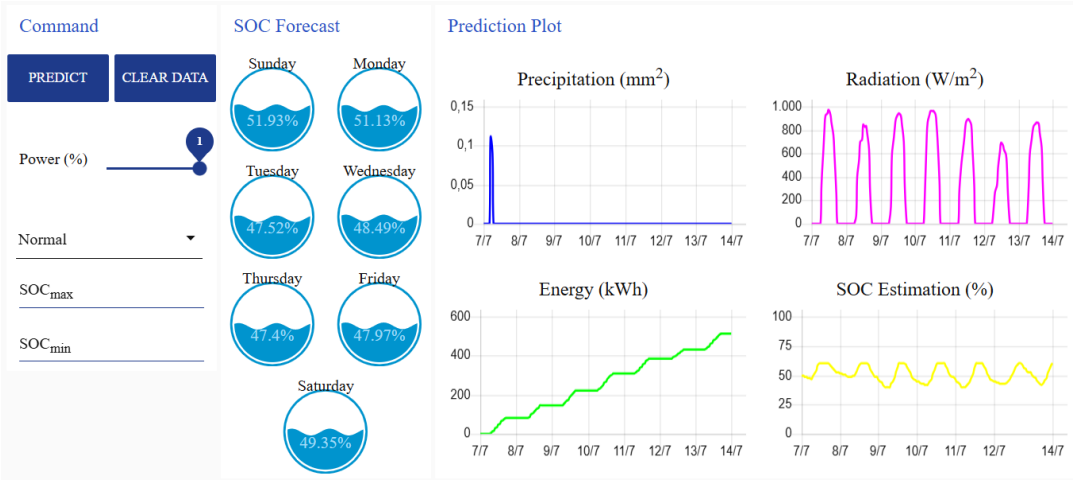

FIGURE 9. User interface created based on the app builder of *Thingable!*. Allows to send commands and monitors the off-grid system.

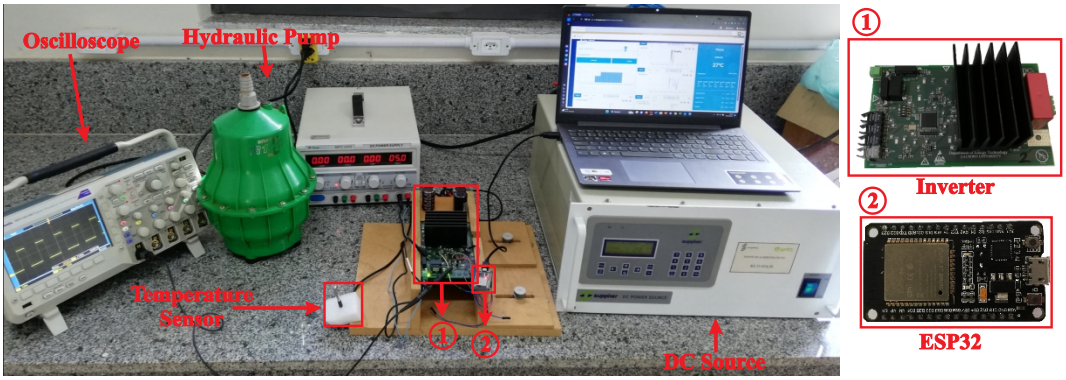

FIGURE 10. Off-grid photovoltaic system experimental setup.

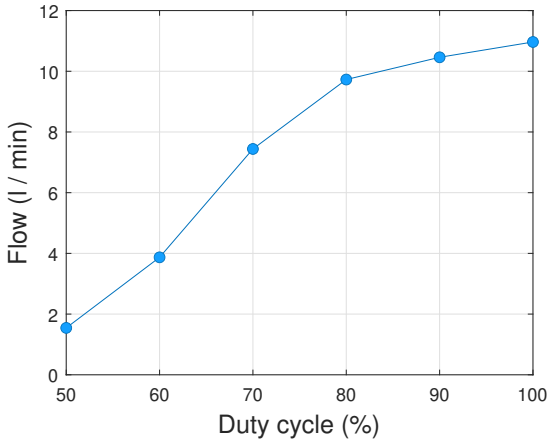

FIGURE 11. Relationship between flow and duty cycle.

while, the ambient temperature is measured by an external sensor using the DS18B20 module, which communicates through a 1-wire bus.

The selected pump for the test is the Anauger R100 vibratory submersible pump [30], it was used in this study due to its compatibility with off-grid photovoltaic systems. The pump nominal power is 175 W. It is a device specifically designed for rural applications, such as water pumping from cisterns, shallow wells, and small-scale irrigation systems."

C. Simulation

The simulation is based on the system depicted in Fig. 1 and the control strategies described in Section II. The parameters used are show in Table 1, including measured values from the pump system.

TABLE 1. Parameters used in the off-grid pump system.

[1.3pt] **Parameter**	**Value**	**Parameter**	**Value**
v_{eq}	86 V	r_{eq}	3.24 Ω
C_{pv}	5 mF	L_{pv}	2 mH
v_{bat}	48 V	R_{bat}	10 mΩ
C_{dc}	1.68 mF	L_{bat}	5 mH
L_{load}	48 mH	R_{load}	1.5 Ω

While the test bench employs a controlled DC source to supply the inverter's DC side, the simulation models the DC link using the control approach outlined in Section II. Additionally, the simulation applies the same modulation

strategy as the test bench, adjusting the pulse width angle to regulate power, as shown in Fig. 11. Furthermore, the pump is represented as an inductive load in the system with values of R_{load} and L_{load}.

IV. RESULTS

A. Test Bench and Simulation Validation

To validate the test bench implementation, it is compared with the simulation to determine whether the comparison is appropriate and the test bench operates as intended. The results considering the voltage and current in the pump are shown in Fig. 12.

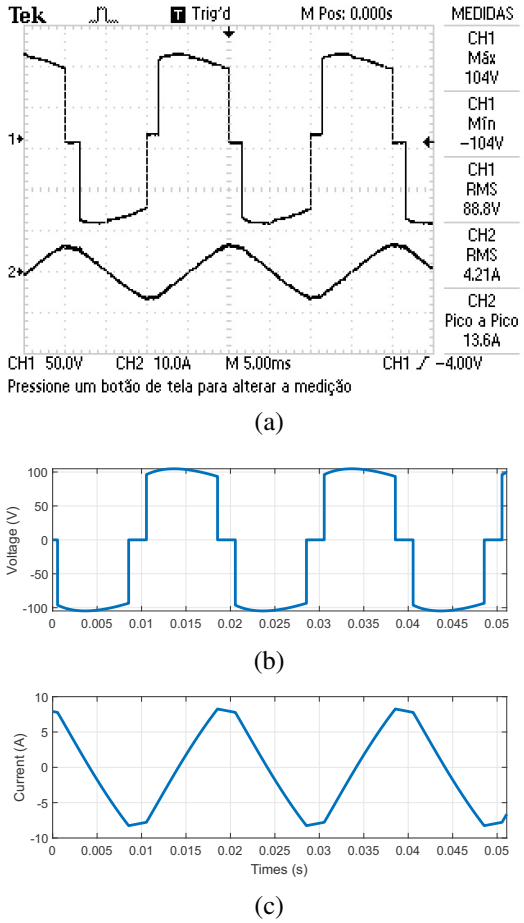

FIGURE 12. Components of the alternating side of the inverter connected to the pump: (a) Voltage and current at the pump terminals, (b) Simulated voltage at the pump terminals, and (c) Current in the pump.

For the validation of the simulation systems with the test bench, a duty cycle value of 0.7 is set for easier comparison. Furthermore, the voltage profile exhibits oscillations at its maximum values during operation due to DC link variations under load. Additionally, the RMS value of the simulated inverter output voltage is 90 V, while the current has an RMS value of 5.5 A. The voltage value suggests that the representation closely matches both signals. However, there is a discrepancy in the pump current, which may indicate that modeling it as a simple resistance and inductance is not entirely appropriate, as it does not account for potential nonlinearities.

Furthermore, the impact in the DC-link is also shown in Fig. 13.

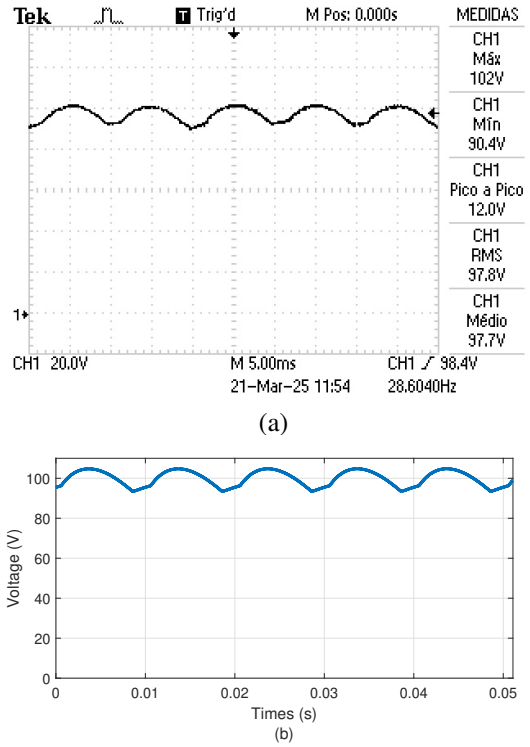

FIGURE 13. Components of the continuous side of the inverter connected to the pump: (a) DC-link voltage and the inverter setup on the test bench. (b) Simulated DC-link voltage.

The average voltage at the DC-link is measured at approximately 98 V, while the simulation and bidirectional boost control ensure a mean value of 100 V. Additionally, the voltage variation is 12 V on the test bench and 11.3 V in the simulation. The RMS value is nearly equal to the mean due to the high magnitude of the average voltage.

B. IoT Validation

To validate the test conditions of the platform, a test was conducted from 9:10 a.m. to 10:10 a.m. The data transmitted to the platform and stored in the database included: the duty cycle command sent by the platform to the pump, the water flow at the pump's output, the inverter DC-link voltage, and the inverter switch temperatures. The stored data are shown in Fig. 14.

This test demonstrates the execution process and the communication between the test bench and the IoT network. Additionally, it is observed that the duty cycle sent to the platform remains around 60%, exhibiting minor fluctuations in accordance with the command. The DC-link voltage maintains a nearly constant value of approximately 100 V, with minimal variation. The water flow varies in response to changes in the duty cycle, with an increase in the duty cycle

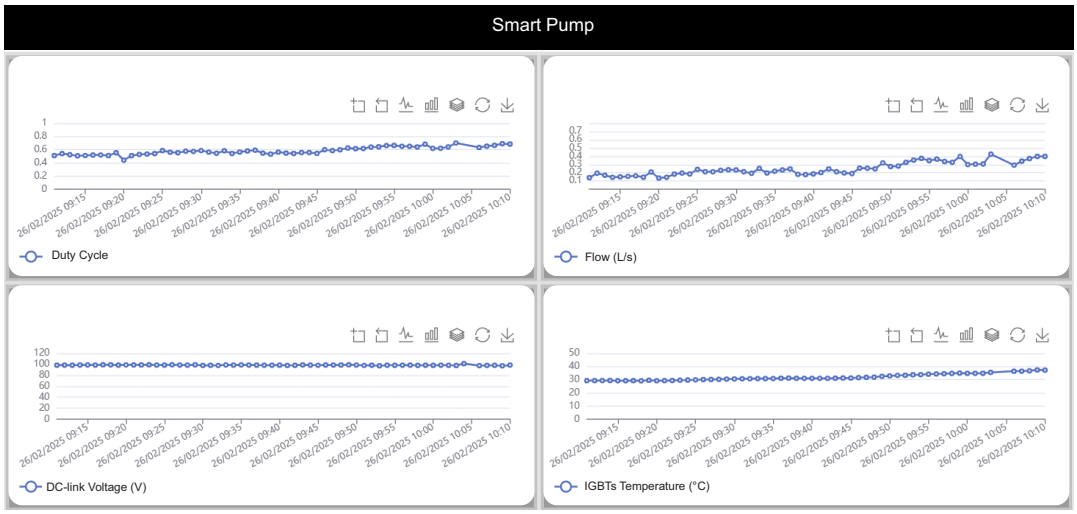

FIGURE 14. Image of the platform data plotted during the extended test.

corresponding to an increase in flow, as shown in Fig. 11. Furthermore, the behavior of the inverter's IGBT is also presented, showing a slight increase in temperature as the operation progresses.

V. CONCLUSION

The proposed system leverages an IoT network to facilitate the integration of a pump with an online platform for monitoring and strategic decision-making. The implementation of the test bench is compared against a simulation that models both buck and boost converters to represent the controlled DC-link voltage source. Additionally, the integration of the Thingable! platform enhances real-time monitoring and control, increasing the system's adaptability by enabling remote adjustments based on weather forecasts and performance metrics.

Experimental validation of the test bench through simulation demonstrated similar results, confirming the accuracy of the system model, except for the pump, which exhibited some discrepancies due to its simplified representation. Performance tests also emphasized the effective communication between system components, with the cloud platform enabling remote control of the water pump's flow rate. The experimental results illustrate the relationship between the duty cycle and flow rate, as well as the system's dynamic response to various commands. Overall, the system's design and integration with IoT technology represent a meaningful advancement in managing off-grid photovoltaic pumping systems, providing enhanced real-time responsiveness.

ACKNOWLEDGMENT

This work was supported in part by Conselho Nacional de Desenvolvimento Científico e Tecnológico (CNPq) (Projects: 307172/2022-8; 407926/2023-2; 443170/2023-1), Coordenação de Aperfeiçoamento de Pessoal de Nível Superior (CAPES), Fundação de Amparo à Pesquisa de Minas Gerais (FAPEMIG) (Projects : RED-00216-23; APQ-03164-24) and INERGE. The authors would also like to thank the CONCERT for the support and for providing access to the *thingable!* platform.

AUTHOR'S CONTRIBUTIONS

L.A.G.LOPES: Conceptualization, Methodology, Validation, Writing – Original Draft. **G.A.CASTRO:** Conceptualization, Investigation, Methodology, Validation, Writing – Original Draft. **D.GONÇALVES:** Conceptualization, Formal Analysis, Investigation, Methodology, Software, Validation, Writing – Original Draft. **R.O.SOUSA:** Conceptualization, Formal Analysis, Methodology, Supervision, Writing – Review & Editing. **A.F.CUPERTINO:** Conceptualization, Funding Acquisition, Investigation, Methodology, Resources, Writing – Review & Editing. **H.A.PEREIRA:** Conceptualization, Formal Analysis, Funding Acquisition, Investigation, Methodology, Resources, Writing – Review & Editing.

PLAGIARISM POLICY

This article was submitted to the similarity system provided by Crossref and powered by iThenticate – Similarity Check.

DATA AVAILABILITY

The data used in this research is available in the body of the document.

REFERENCES

[1] K. Kaygusuz, "Energy for sustainable development: A case of developing countries", *Renewable and Sustainable Energy Reviews*, vol. 16, no. 2, pp. 1116–1126, 2012, doi:10.1016/j.rser.2011.11.013.

[2] Instituto Estadual de Meio Ambiente e Recursos Hídricos , "Soluções em Meio Ambiente", Accessed on July 08, 2024, URL: https://iema.es.gov.br/Media/iema/CQAI/EIA/2003/PCH%20Timbu%C3%AD%20Seco/D-I-_-Introdu%C3%A7%C3%A3o.pdf.

[3] International Energy Agency (IEA), "Energy Access", Accessed on July 08, 2024, 2022, URL: https://www.iea.org/topics/energy-access.

[4] S. Feron, "Sustainability of Off-Grid Photovoltaic Systems for Rural Electrification in Developing Countries: A Review", *Sustainability*, vol. 8, no. 12, 2016, doi:10.3390/su8121326.

[5] O. Rigovacca, S. Polimeni, G. Manzolini, S. Leva, P. Raboni, "Analyses of Electrification and Battery Ageing Processes in a Real Offgrid Hybrid Microgrid", *in 2019 IEEE Milan PowerTech*, pp. 1–6, 2019, doi:10.1109/PTC.2019.8810990.

[6] A. ur Rehman, M. T. Iqbal, "Design and Control of an Off-Grid Solar System for a Rural House in Pakistan", *in 2020 11th IEEE Annual Information Technology, Electronics and Mobile Communication Conference (IEMCON)*, pp. 0786–0790, 2020, doi:10.1109/IEMCON51383.2020.9284867.

[7] S. Gutiérrez, "Prototype for an off-grid photovoltaic system with low cost solar tracking", *in 2017 IEEE Mexican Humanitarian Technology Conference (MHTC)*, pp. 7–11, 2017, doi:10.1109/MHTC.2017.7926198.

[8] R. C. de Barros, W. C. S. Amorim, W. d. C. Boaventura, A. F. Cupertino, V. F. Mendes, H. A. Pereira, "Methodology for BESS Design Assisted by Choice Matrix Approach", *Eletrônica de Potência*, vol. 29, p. e202412, Jun. 2024, doi:10.18618/REP.2005.1.019027.

[9] M. Rezkallah, A. Chandra, M. Saad, M. Tremblay, B. Singh, S. Singh, H. Ibrahim, "Design and Implementation of Decentralized Control for Distributed generation based Off-grid System", *in 2020 IEEE International Conference on Power Electronics, Smart Grid and Renewable Energy (PESGRE2020)*, pp. 1–6, 2020, doi:10.1109/PESGRE45664.2020.9070284.

[10] M. Khatami, H. Mortazavi, M. R. Mashhadi, M. Oloomi, "Designing an off-grid PV system: For a residential consumer in Mashhad-Iran", *in 2013 Africon*, pp. 1–5, 2013, doi:10.1109/AFRCON.2013.6757680.

[11] A. A. Dionizio, L. P. Sampaio, S. A. O. d. Silva, "Inversor Integrado Zeta para Aplicações em Sistemas Autonômos Monofásicos de Geração de Energia", *Eletrônica de Potência*, vol. 27, no. 4, p. 313–324, Oct. 2022, doi:10.18618/REP.2022.4.0016.

[12] F. A. Fairuz, N. Sartika, L. Kamelia, A. E. Setiawan, S. Bilqis, A. Ramelan, "Monitoring of Off-grid Solar Power Plant Prototype for Residential Loads Based on Internet of Things", *in 2023 10th International Conference on Electrical Engineering, Computer Science and Informatics (EECSI)*, pp. 98–103, 2023, doi:10.1109/EECSI59885.2023.10295932.

[13] T. Logenthiran, D. Srinivasan, A. M. Khambadkone, H. N. Aung, "Multiagent System for Real-Time Operation of a Microgrid in Real-Time Digital Simulator", *IEEE Transactions on Smart Grid*, vol. 3, no. 2, pp. 925–933, 2012, doi:10.1109/TSG.2012.2189028.

[14] D. Gebbran, A. Barragán-Moreno, P. I. Gómez, R. K. Subroto, M. M. Mardani, M. López, J. Quiroz, T. Dragičević, "Cloud and Edge Computing for Smart Management of Power Electronic Converter Fleets: A Key Connective Fabric to Enable the Green Transition", *IEEE Industrial Electronics Magazine*, vol. 17, no. 2, pp. 6–19, 2023, doi:10.1109/MIE.2022.3211125.

[15] N. M. Kumar, K. Atluri, S. Palaparthi, "Internet of Things (IoT) in Photovoltaic Systems", *in 2018 National Power Engineering Conference (NPEC)*, pp. 1–4, 2018, doi:10.1109/NPEC.2018.8476807.

[16] S. H. Jeon, J. Lee, J. K. Choi, "Energy Outage-Aware Power Distribution Scheme for Off-Grid Base Station Operation", *IEEE Communications Letters*, vol. 21, no. 6, pp. 1401–1404, 2017, doi:10.1109/LCOMM.2017.2676108.

[17] S. M. A. A. Abir, A. Anwar, J. Choi, A. S. M. Kayes, "IoT-Enabled Smart Energy Grid: Applications and Challenges", *IEEE Access*, vol. 9, pp. 50961–50981, 2021, doi:10.1109/ACCESS.2021.3067331.

[18] C. Essayeh, M. Raiss El-Fenni, H. Dahmouni, "Load management strategy for an OFF-grid switched mode in smart Micro-Grid systems", *in 2016 International Conference on Wireless Networks and Mobile Communications (WINCOM)*, pp. 52–57, 2016, doi:10.1109/WINCOM.2016.7777190.

[19] B. S. Sami, "Intelligent Energy Management for Off-Grid Renewable Hybrid System Using Multi-Agent Approach", *IEEE Access*, vol. 8, pp. 8681–8696, 2020, doi:10.1109/ACCESS.2019.2963584.

[20] M. Jafari, Z. Malekjamshidi, J. Zhu, M.-H. Khooban, "A Novel Predictive Fuzzy Logic-Based Energy Management System for Grid-Connected and Off-Grid Operation of Residential Smart Microgrids", *IEEE Journal of Emerging and Selected Topics in Power Electronics*, vol. 8, no. 2, pp. 1391–1404, 2020, doi:10.1109/JESTPE.2018.2882509.

[21] A. Azeem, I. Ismail, S. M. Jameel, V. R. Harindran, "Electrical Load Forecasting Models for Different Generation Modalities: A Review", *IEEE Access*, vol. 9, pp. 142239–142263, 2021, doi:10.1109/ACCESS.2021.3120731.

[22] M. Jafari, Z. Malekjamshidi, D. D.-C. Lu, J. Zhu, "Development of a Fuzzy-Logic-Based Energy Management System for a Multiport Multioperation Mode Residential Smart Microgrid", *IEEE Transactions on Power Electronics*, vol. 34, no. 4, pp. 3283–3301, 2019, doi:10.1109/TPEL.2018.2850852.

[23] G. A. Castro, L. A. Gregório Lopes, D. Gonçalves, R. O. De Sousa, A. F. Cupertino, H. A. Pereira, "Can Off-Grid System be Improved to be Smart? How Internet of Things can Change the Game", *in 2023 IEEE 8th Southern Power Electronics Conference and 17th Brazilian Power Electronics Conference (SPEC/COBEP)*, pp. 1–6, 2023, doi:10.1109/SPEC56436.2023.10407989.

[24] CONCERT Technologies, "thingable! IoT Platform", https://www.thingable.com.br, access on May 30, 2025.

[25] M. Villalva, T. Siqueira, E. Filho, "Voltage Regulation of Photovoltaic Arrays: Small-Signal Analysis and Control Design", *Power Electronics, IET*, vol. 3, pp. 869 – 880, 12 2010, doi:10.1049/iet-pel.2008.0344.

[26] M. G. Villalva, E. Ruppert Filho, "Dynamic analysis of the input-controlled buck converter fed by a photovoltaic array", *Sba: Controle & Automação (Sociedade Brasileira de Automática)*, vol. 19, no. 4, pp. 463–473, 12 2008, doi:10.1590/S0103-17592008000400009.

[27] A. F. Cupertino, H. A. Pereira, V. F. Mendes, "Modeling, Design and Control of a Solar Array Simulator Based on Two-Stage Converters", *Journal of Control, Automation and Electrical Systems*, vol. 28, no. 5, pp. 585–596, Oct. 2017, doi:10.1007/s40313-017-0333-z.

[28] D. Hart, *Eletrônica de Potência: Análise e Projetos de Circuitos*, McGraw Hill Brasil, 2016.

[29] National Renewable Energy Laboratory, "Developer Network", https://developer.nrel.gov, access on July 30, 2024.

[30] Anauger, "ANAUGER® Solar R100", Access on Juny 18, 2025.

BIOGRAPHIES

Luis Antonio Gregório Lopes is native of São Miguel do Anta, Minas Gerais, born in 2003. Currently an undergraduate student in Electrical Engineering (since 2021) at the Federal University of Viçosa – UFV, and a CNPq Scientific Initiation scholarship holder through GESEP (2022–2025).

Giovani Aneres Castro is an undergraduate student in Electrical Engineering at the Federal University of Viçosa (UFV). He has earned two OBMEP medals and participated four times in the OBMEP Scientific Initiation Program. He conducted research projects in physics (2018) and mathematics (2020–August 2022), focusing on colloidal quantum dots and partial differential equations, respectively. He is currently a member of the Gerência de Especialistas em Sistemas Elétricos de Potência (GESEP). His main research interests include calculating magnetic losses and characterizing electrical steels.

Diuary Gonçalves received the B.S. degree in electrical engineering from the Universidade Federal de Viçosa, Viçosa, Brazil, in 2022, and the M.S. degree in electrical engineering from the Centro Federal de Educação Tecnológica of Minas Gerais, Belo Horizonte, Brazil, in 2023. Currently doing his Ph.D. degree in electrical engineering from the Federal Center for Technological Education of Minas Gerais, Belo Horizonte, Brazil. He is currently a Federal Institute Professor at the Department of Electrical Engineering, Centro Federal de Educação Tecnológica Celso Suckow da Fonseca - Nova Friburgo, Rio de Janeiro, Brazil. His main research interests include battery energy storage systems, battery state of health and charge estimation, and photovoltaic inverter control and modelling.

Renata Oliveira de Sousa received the B.S. degree in electrical engineering from the Federal University of Viçosa, Viçosa, Brazil, in 2018, the M.S. degree in electrical engineering from the Federal Center for Technological

Education of Minas Gerais, Belo Horizonte, Brazil, in 2019, and the Ph.D. degree in electrical engineering from the Federal University of Minas Gerais, Belo Horizonte, in 2022. From 2021 to 2022, she was a Guest Ph.D. student with the Department of Energy, Aalborg University, Aalborg, Denmark. From 2020 to 2021, she was a Adjunct Professor with the Department of Electrical Engineering, Federal Center for Technological Education of Minas Gerais. She is currently an Assistant Professor at the Department of Electronics, Federal University of Technology - Paraná, Curitiba, Brazil. She is a member of the Brazilian Power Electronics Society (SOBRAEP). Her main research interests include the reliability of power electronics-based systems, multilevel converters, smart battery-based storage systems, and fiber optic instrumented systems.

Allan Fagner Cupertino received the Bachelor's degree in Electrical Engineering from the Federal University of Viçosa in 2013, and the Master's and Doctoral degrees in Electrical Engineering from the Federal University of Minas Gerais in 2015 and 2019, respectively. Was a visiting Ph.D. student at the Department of Energy Technology at Aalborg University from 2018 to 2019. From 2014 to 2022, was an Assistant Professor at the Federal Center for Technological Education of Minas Gerais. Since 2023, has been with the Department of Electrical Energy at the Federal University of Juiz de Fora. His main research interests include renewable energy conversion systems, smart battery energy storage systems, cascaded multilevel converters, and reliability. Prof. Cupertino was awarded the President Bernardes Silver Medal in 2013, the SOBRAEP Doctoral Thesis Award in 2020, and the IAS CMD Doctoral Thesis Contest in 2021. He is a member of the Brazilian Power Electronics Society and the Brazilian Society of Automatics.

Heverton Augusto Pereira obtained the Bachelor's degree in Electrical Engineering from the Federal University of Viçosa, Brazil, in 2007, the Master's degree from the State University of Campinas in 2009, and the Doctoral degree from the Federal University of Minas Gerais in 2015, all in the field of Electrical Engineering. Was a visiting researcher at the Department of Energy Technology at Aalborg University, Denmark, in 2014. Has been working as an Associate Professor in the Department of Electrical Engineering at UFV since 2009. His main research interests include grid-connected converters for solar energy systems and energy storage systems.